Biophysical Journal
Article

Biophysical Society

Structural Behavior of the Peptaibol Harzianin HK VI in a DMPC Bilayer: Insights from MD Simulations

Marina Putzu,[1] Sezgin Kara,[2] Sergii Afonin,[3] Stephan L. Grage,[3] Andrea Bordessa,[4] Grégory Chaume,[4] Thierry Brigaud,[4] Anne S. Ulrich,[2,3] and Tomáš Kubař[1,*]

[1]Center for Functional Nanostructures and Institute of Physical Chemistry, [2]Institute of Organic Chemistry, and [3]Institute of Biological Interfaces (IBG-2), Karlsruhe Institute of Technology, Karlsruhe, Germany; and [4]Laboratoire de Chimie Biologique (LCB), EA 4505, Université de Cergy-Pontoise, Neuville sur Oise, Cergy-Pontoise Cedex, France

ABSTRACT Microsecond molecular dynamics simulations of harzianin HK VI (HZ) interacting with a dimyristoylphosphatidylcholine bilayer were performed at the condition of low peptide-to-lipid ratio. Two orientations of HZ molecule in the bilayer were found and characterized. In the orientation perpendicular to the bilayer surface, HZ induces a local thinning of the bilayer. When inserted into the bilayer parallel to its surface, HZ is located nearly completely within the hydrophobic region of the bilayer. A combination of solid-state NMR and circular dichroism experiments found the latter orientation to be dominant. An extended sampling simulation provided qualitative results and showed the same orientation to be a global minimum of free energy. The secondary structure of HZ was characterized, and it was found to be located in the 3_{10}-helical family. The specific challenges of computer simulation of nonpolar peptides are discussed briefly.

INTRODUCTION

Peptaibols

Peptaibols are a special class of short peptides with a length from seven to twenty amino acids (AA), significant content of noncanonical α-tetrasubstituted residues like the aminoisobutyric acid (Aib), alkylated N-terminus, and a C-terminal 1,2-amino alcohol group (1). Largely hydrophobic and proteolytically stable, nonribosomally produced peptaibols are secondary metabolites in soil filamentous fungi and demonstrate pronounced antibiotic, antifungal, and anticancer activities, which render them as potentially interesting leads for pharmacological and agricultural applications. Peptaibols are uniformly membrane-active compounds, and like many other membranolytic peptides, they are believed to exert their activity mostly via a pore formation in targeted biomembranes. In this connection, peptaibols are particularly intriguing membrane-active peptides (MAP) because many of them indeed show membrane voltage activation and formation of ionic channels in artificial lipid bilayers. Hence, peptaibols have been much investigated as model systems for voltage-gated phenomena.

The backbone of a peptaibol molecule generally forms a helical structure due to the conformational constraints imposed by the presence of abundant Aib (2). Homooligomeric Aib peptides prefer the 3_{10}-helical conformation whereas either α- or mixed-helical conformations prevail whenever Aib is incorporated as a guest residue in host polypeptides (3–6). Furthermore, the helix-stabilizing effect of Aib in a foreign sequence even overrides the effects of helix-breaking AAs (3). Peptaibols are classified into: 1) long-sequence peptaibols (18–20 AA, typically with a centrally located Pro, and Gln residues near both termini); 2) short-sequence peptaibols (11–16 AA, with several Aib-Pro motives, and typically either Ac-Aib-Asn- or Ac-Aib-Gln- as N-terminus); and 3) ultrashort lipopeptaibols (7 or 11 AA, with a high content in Gly and N-terminal AA acylated by a C8–C15 fatty acid).

The archetypal representatives of the long-sequence peptaibols are alamethicins (ALM). The most studied variant ALM F30/3 (Ac-Aib-Pro-Aib-Ala-Aib-Ala-Gln-Aib-Val-Aib-Gly-Leu-Aib-Pro-Val-Aib-Aib-Glu-Gln-Pheol) forms amphipathic α-helices, which assemble into stable ion channels with well-defined conductance levels, and its resultant cytolytic activity was recognized already in the 1960s (7). ALM may either bind to the surface of a lipid bilayer, or it may penetrate into the interior of the bilayer; as soon as inserted, it may form oligomers and, thus, create barrel-stave or helix-bundle channels (8,9), which may be filled with water and conduct ions consequently. Short-sequence peptaibols were also reported to form pores and channels

Submitted December 14, 2016, and accepted for publication May 12, 2017.

*Correspondence: tomas.kubar@kit.edu

Editor: Bert de Groot.

http://dx.doi.org/10.1016/j.bpj.2017.05.019

on planar lipid bilayer membranes (10). However, most of the studies of short-sequence peptaibols have focused on solution structural features, and not so much is known as for the behavior of these peptaibols inside a membrane. On the contrary, lipopeptaibols received more attention with regard to the membrane-inserted structure. Representative is the lipopeptaibol trichogin GA IV of the sequence nOct-Aib-Gly-Leu-Aib-Gly-Gly-Leu-Aib-Gly-Ile-Leuol (11).

Harzianin HK VI

The subject of this work is the short-sequence peptaibol harzianin HK VI (hereafter called "HZ"). HZ is produced naturally by various terrestrial and marine fungi of the *Trichoderma sp.*, and was first isolated from *T. pseudokoningii* and characterized by Rebuffat et al. (12) in 1996. Within its 11-residue sequence, Ac-Aib-Asn-Ile-Ile-Aib-Pro-Leu-Leu-Aib-Pro-Leuol, HZ contains two Aib-Pro pairs at positions 5–6 and 9–10, the Ac-Aib-Asn run at the N-terminus, and several bulky hydrophobic Leu/Ile residues. Notably, due to mass spectrometry being the prime sequencing method, inability to distinguish Leu from Ile leads to the ambiguity in identification of HZ analogs, e.g., when Lxx is reported as an aliphatic residue.

Functional studies showed HZ, its homologs (Ac-Aib-Asn-Lxx-Lxx-Aib-Pro-Lxx-Lxx-Aib-Pro-Lxxol), or mixtures containing HZ to exert embryotoxicity against *Crassostrea gigas* (13) as well as chlorpromazine-level neuroleptic effects in male mice (14). Crude extracts from HZ-producing fungi inhibited motility of the boar spermatozoa and quenched the mitochondrial transmembrane potential of the sperm cells at low exposure concentrations (14,15). HZ is a membrane-active peptaibol as it was reported to cause leakage of the carboxyfluorescein-loaded lecithin/cholesterol liposomes and, as other short-sequence peptaibols, forms pores and channels on planar lipid bilayer membranes (10,12,15). HZ can act as a cell-penetrating peptide—uptake of covalently conjugated oligonucleotides was shown (16,17).

Notably, there are no particularly strong in vitro cytotoxic effects demonstrated specifically for HZ or any other short-sequence peptaibols. Taken together with the fact that peptaibols are produced in mixtures as natural combinatorial libraries, this finding challenges putative exclusive membranolytic cytotoxicity as a prime mechanism of biological action and the main purpose of their biosynthetic production. Particularly interesting as alternatives are recently suggested synergies between hydrolytic enzymes and membrane-affecting peptaibols indirectly leading to concerted fungicidal effects (18). Furthermore, a 2012 article by Mikkola et al. (15) proposes the synergistic enhancement of the membrane-permeabilizing activity of canonical 20-mer peptaibols (like ALM) by the 11-mer ones, i.e., by the short-sequence peptaibols like HZ. Should any of these alternatives or the direct membranolytic action be the prime mechanism of HZ biological action, determination of HZ structure in the membrane-bound state is of key relevance.

From the general structure perspective, all harzianins (and their sequential analogs) including HZ were suggested to assume a β-bend ribbon spiral secondary structure, based on partial NMR structural studies of HZ and compositional homology to other (longer) harzianins. The β-bend ribbon conformation with backbone torsion angles as in Table 1 (19) was determined in MeOH using CD, molecular modeling, and NMR for the 14-mer harzianin HC IX. For this harzianin, the β-bend ribbon spiral was stabilized by type 1 $\leftarrow$ 4 intramolecular H-bonds, some of which were absent in accordance with the presence of three Pro residues interrupting the hydrogen-bonding (H-bonding) network. The β-bend ribbon structure is logically projected to all $(\text{Aib-Pro})_n$- and Xaa-Yaa-Aib-Pro-containing peptides in parallel to the expectation of a 3_{10}-helix for any oligo-Aib sequence. (Both compositional characteristics are present in HZ.) At the same time, an α-helical assumption appears not to be relevant for HZ, as it seems to prevail only for Aib-poor long-sequence peptaibols like ALMs.

Simulation of membrane-active peptides

Molecular dynamics (MD) simulation has been a useful tool for the investigation of MAPs for two decades. A comprehensive how-to on MD simulations of membrane proteins by Kandt et al. (20) and a short review by Lindahl and Sansom (21) cover also MAPs. MD simulations of MAPs face multiple challenges regarding the parametrization of lipids or more generally the development of force fields uniform for bilayers and molecules embedded into them, or the principal limitations of potential energy functions lacking electronic polarizability (22–24). Even if these challenges are tackled, there is a real danger of undersampling in all-atom MD simulations of even simple peptide-bilayer systems, as noted in the late 1990s already (25–27), and discussed, e.g., in Lindahl and Sansom (21). The reason is that the hydrocarbon tails of lipids rearrange very slowly; as an illustration, note the (lateral) diffusion coefficient in DMPC of 1–10 $\mu m^2/s$ (28,29), as compared to the value for water of 2000–3000 $\mu m^2/s$ (30).

A partial solution of this problem is to pass to coarse-grained (CG) representation (31), e.g., with the Martini force field (32), which improves the sampling by a factor of 100–1000. That makes CG simulation undoubtedly

TABLE 1 Backbone Dihedral Angles of the Fragment Forming a β-bend Ribbon Spiral Structure

Residue	φ	ψ
Xaa (i)	$(-90 \pm 8)^\circ$	$(-27 \pm 18)^\circ$
Yaa ($i+1$)	$(-98 \pm 11)^\circ$	$(-17 \pm 14)^\circ$
Aib ($i+2$)	$(-49 \pm 3)^\circ$	$(-50 \pm 1)^\circ$
Pro ($i+3$)	$(-78 \pm 1)^\circ$	$(+3 \pm 19)^\circ$

Data is from Ségalas et al. (19).

useful for the initial docking and refinement of orientation with low resolution at least, whereas the lower level of detail may be of limited use for complex lipid environments, specific interactions, and fine conformational changes (31).

A promising simulation strategy seems to be to combine CG and all-atom representations for large-scale sampling and more detailed description of relevant structural states, respectively, to take advantage of the strengths of both of the approaches, as described by Rzepiela et al. (33). Parton et al. (34) exploited such a multiscale idea, starting with a CG simulation, then converting to an all-atom representation, and simulating further with an all-atom force field. Similarly, studying antimicrobial lipopeptides, Horn et al. (35) applied all-atom simulations to characterize the structural perturbation of the membrane, whereas they examined the (slow) process of binding to the membrane with a CG model (36).

Generally, the reliability and suitability of MD simulation should be tested by comparison with the outcome of biophysical experiments, like in the dedicated study by Wang et al. (37). The factors that affected the quality of the results were mostly the choice of the force field and the simulation parameters like inclusion or omission of counterions and the treatment of long-range electrostatics. These important topics were discussed also in other publications (38,39).

MAPs have been also a subject of work applying advanced simulation techniques. The temperature replica exchange protocol (replica-exchange MD) (40) was exploited in structural studies (41–44). The dissipative particle dynamics (45), which is a variant of CG MD, was applied in a study of pore formation and other bilayer deformations caused by several different MAPs (46). Umbrella sampling with a novel reaction coordinate was used in a work on antimicrobial lipopeptides forming a micelle and fusing with a membrane (47). Finally, a series of modern techniques were employed in a thermodynamic study of the WALP peptide (48): replica-exchange MD was combined with metadynamics with newly designed collective variables to yield the free energy of folding, and CG simulations used the Hamiltonian replica-exchange approach (HREX). These studies illustrate the flexibility and the broad range of options available for MD simulations of peptide/bilayer complexes.

Simulation of peptaibols

Approaching the topic of this work, MD simulations were previously employed to investigate the interaction of the long-sequence peptaibol ALM with lipid bilayers mostly consisting of POPC. Sometimes, ALM channels were built artificially first, and then simulated over tens of nanoseconds. The stability and dynamics properties of the helical bundles, the secondary structural elements, as well as the intra- and intermolecular H-bonding patterns were examined. First, rather short, all-atom simulations concentrated on a single ALM molecule, its structural stability, and insertion pathway (27,49), and the latter point was analyzed in longer simulations (50). Further studied was the aggregation of several ALM molecules to form channels (51), a complex topic that was also approached with a combination of CG and all-atom simulations (52). The formation of aggregates was simulated on a CG level, and then all-atom simulations were applied to focus on the secondary structure of ALM as well as the interaction of water with the ALM clusters. The structure of the clusters was rather irregular, different from previous suggestions of symmetric channels formed by perfect α-helices. The observations would not have been possible with either CG or all-atom simulations alone.

Regarding short-sequence peptaibols, of which HZ is a representative, not much simulation work seems to have been done. Merely conformational analyses of short-sequence peptaibols in aqueous solution were reported, investigating trichobrachin A and B (53) and hypomurocin A (54). Further, an MD simulation study of the lipopeptaibol trichogin GA IV showed that such a short lipidated molecule interacts better with bilayers that are thinner by themselves, or, alternatively, the binding of the lipopeptaibol may induce local thinning of the membrane (55). It was noted, however, that the extent of simulation was insufficient to obtain global thermodynamics equilibrium due to the slow lateral diffusion of the lipid.

Aim of this work

The aim of this work is to simulate, for the first time to our knowledge, an entirely nonpolar peptide, a short-sequence peptaibol interacting with a lipid bilayer under conditions of low P/L. The primary goals are 1) to determine the mode of interaction of HZ with the bilayer by combination of the simulations with NMR experiments and 2) to establish the secondary structure on the basis of the simulations, also producing structural models for a subsequent solid-state NMR analysis. This will provide a comprehensive picture of the HZ molecule interacting with a DMPC bilayer at low P/L. In addition, free energies of the different possible orientations of HZ will be estimated. Also demonstrated will be any possible difficulties and challenges of application of MD simulation for such a system involving a nonpolar peptide, as opposed to applications to more usual polar or cationic peptides.

MATERIALS AND METHODS

Force fields, general simulation parameters, and starting structures

The molecular system to be simulated consisted of one HZ molecule of the sequence Ac-Aib-Asn-Ile-Ile-Aib-Pro-Leu-Leu-Aib-Pro-Leuol, a bilayer formed by 128 DMPC molecules, and ~3500 water molecules. The system was enclosed in a rectagonal periodic box sized $\sim 6.3 \times 6.3 \times 6.0$ nm^3. In the simulation with HZ starting outside the bilayer, the box size was increased by ~1 nm in the direction of the bilayer normal (z), and the number of water molecules was increased to 4300. A combination of the

following force fields was used to describe the system: Amber parm14SB (56–58) for the HZ molecule, slipids (59–61) for the DMPC molecules, and TIP3P (62) for the water.

All of the simulations were performed with the Gromacs package, versions 5.0.1 and 4.6.7 (63,64). The cumulative sampling in this study amounts to 32 μs for the simulations presented in the main text (16 μs of free simulations and 16 μs of HREX), and 72 μs for the additional simulations reported in the Supporting Material (8 μs of HREX, 4 μs of metadynamics, and 60 μs of umbrella sampling). These are state-of-the-art timescales, approaching those in contemporary supercomputer studies of other authors like, e.g., that in Wang et al. (65).

Additional details can be referred to in the Supporting Material.

Free MD simulations

A series of free MD simulations of HZ molecule interacting with the DMPC bilayer was performed, considering four different continuous initial conformations of the peptide: the α-helix, the 3_{10}-helix, the β-bend ribbon helix, and the fully extended conformation. Some simulations involved additional restraints to keep the conformation of HZ close to the initial one, as detailed in the Supporting Material.

Restrained simulations were performed with three different initial conformations (which were also reference conformations for the restraints, at the same time): the α-helix, the 3_{10}-helix, and the β-bend ribbon. Unrestrained simulations were performed with two different initial conformations, the 3_{10}-helix and the fully extended conformation. For each of these five options regarding the conformation of HZ molecule, three different initial positions/orientations were considered: 1) HZ in the aqueous solvent, subject to heating-cooling protocol (see the Supporting Material) subsequently; 2) HZ inside the bilayer, with its molecular axis perpendicular to the bilayer surface; and 3) HZ inside the bilayer, immersed in the hydrophobic region, with the HZ axis parallel to the bilayer surface. Thus, in total 15 individual free MD simulations were performed, and every of them was extended to 1 μs.

In addition, a cationic analog of HZ interacting with the DMPC bilayer was simulated. That peptide had an AA sequence Ace-Aib-Asn-Lys-Lys-Aib-Pro-Lys-Lys-Aib-Pro-Leuol and will be referred to as "HZ^{4+}". Its initial conformation was considered to be 3_{10}-helical, and the starting structure of the complete system was constructed with the heating-cooling protocol (see the Supporting Material). Then, an unrestrained MD simulation of 1 μs was performed.

HREX

The replica-exchange method with solute tempering REST2 (66) was applied as implemented in Plumed 2.1.2 (67) interfaced to Gromacs 4.6.7. An HREX simulation was performed with eight replicas, in which the scaling factor λ followed a geometric series in the range of 1–0.3, corresponding to effective temperatures of 300–1000 K. The amplitudes of dihedrals in the HZ molecule were scaled by λ, and for the nonbonded interactions, the charges and Lennard-Jones depths of the atoms of HZ were scaled by $\sqrt{\lambda}$ and λ, respectively. The HREX simulation ran for 2 μs, exchange was attempted every 2 ps for neighboring replicas, and the atomic coordinates were saved every 20 ps. The simulation was started with a 3_{10}-helical HZ molecule placed inside the DMPC bilayer, with its helical axis perpendicular to bilayer surface. No barostat was applied in the HREX simulations, thus an NVT canonical ensemble was sampled.

The trajectory generated by the unperturbed replica (scaling factor of one) was used to generate a plot of free energy as a function of two variables. These two collective variables were defined in the Cartesian coordinate system, with the DMPC bilayer oriented in the xy plane and the z axis being perpendicular to it, in the following way: The first variable was the distance in the z direction (i.e., projection of the distance on the z axis) between the center of mass (COM) of the HZ molecule and the COM of all lipid atoms of the entire bilayer. The second variable was the angle between the major axis of the HZ molecule, and the z axis. To obtain the axis vector of HZ, the backbone atoms of HZ (all of the N, Cα, C_{co}, and O atoms) were divided into two equally sized groups, one being N-terminal and the other being C-terminal, and a COM was obtained for each of them, $\vec{R}(\mathrm{N})$ and $\vec{R}(\mathrm{C})$. The helix axis was considered to pass through these two COMs, $\vec{R}(\mathrm{NC}) = \vec{R}(\mathrm{C}) - \vec{R}(\mathrm{N})$. Finally, the tilt angle was obtained from the z component of $\vec{R}(\mathrm{NC})$ as $\tau = \arccos(R_z(\mathrm{NC})/R(\mathrm{NC}))$. The two-dimensional space in z and τ was divided into equally spaced bins of width of 0.20 Å and 1.1°, respectively, and the occurrences of (z,τ) from the replicas running with the unperturbed Hamiltonian were counted. The resulting probability distributions $\mathcal{P}(z,\tau)$ were recalculated to free energies as $\Delta G = -k_B T \log(\mathcal{P})$, with k_B being the Boltzmann constant and $T = 300$ K.

Experimental work

The description of the methodology can be referred to in the Supporting Material.

RESULTS

Orientation of HZ from MD simulations

All-atom MD simulations were performed for one HZ molecule interacting with a DMPC bilayer. Fifteen independent trajectories over 1 μs were generated, using different initial conformations, positions, and orientations of HZ in the bilayer. Some of the simulations employed distance or dihedral restraints to force a given secondary structure of the HZ molecule. The HZ molecule was always found embedded into the lipid bilayer in every simulation, and the dominant orientation observed in each of the simulations is presented in Table 2.

A striking observation is that each of the many simulations started from different initial conditions converged to one of just two distinct structures. In what follows, these will be designated as the S-state—the HZ molecule is in the interfacial layer between the nonpolar and headgroup regions of the bilayer, with its main axis parallel to the bilayer

TABLE 2 Resulting Orientation of HZ in Each of the Individual Free MD Simulations Performed with the Different Initial Conditions

		Initial Position of HZ		
			In Bilayer:	In Bilayer:
Initial Conformation	Restraints	In Solvent	HZ Axis to Bilayer Plane Initially Parallel	HZ Axis to Bilayer Plane Initially Perpendicular
α-helix	α	S	I	I
3_{10}-helix	3_{10}	I	I	I
β-bend ribbon	β-bend	I	I	I
Fully extended	none	S	S	I
3_{10}-helix	none	S*	S	I*

S, surface-bound orientation with HZ at the inner edge of the bilayer surface and the HZ axis parallel to the surface; I, transmembrane orientation with HZ axis perpendicular to the bilayer surface; the asterisks represent MD trajectories considered in the following analyses.

surface; and the I-state—the HZ molecule spans most of the hydrophobic bilayer width, with its main axis perpendicular to the bilayer surface. The representative instances of the S- and I-states are shown in Fig. 1.

It is also interesting that the outcome of MD simulations is different whenever the conformation of the HZ molecule is restrained to a certain structure by means of distance restraints imposed on H-bonds or backbone dihedral angles. Specifically, all of the simulations with HZ restrained to 3_{10}-helical or β-bend conformation actually led to an I-state orientation of HZ, no matter what the initial orientation in the simulation was. Thus, it seems that the flexibility of the HZ molecule may play a certain role in either the relative propensities of the different orientations or the process of insertion of HZ into the membrane.

All of the structural analyses below are based on the trajectories from two of the performed MD simulations, marked with asterisks in Table 2; these were unrestrained simulations with the HZ molecule in a 3_{10}-helical structure initially, placed either inside the bilayer perpendicular to its surface, which led to the I-state, or outside of the membrane and subjected to a heating-cooling protocol, which provided the S-state. Additionally, a simulation of a hypothetical charged mutant of HZ in an orientation resembling the S-state was performed. This molecule, HZ^{4+}, has Ile^{3}, Ile^{4}, Leu^{7}, and Leu^{8} replaced by lysines and carries four positive charges. To analyze the location of the peptide molecule within the bilayer in the different states in more detail, one-dimensional densities of atoms across the bilayer were obtained from MD trajectories (see Fig. 2). Also, the flexibility of conformation of the HZ molecule was quantified by means of the root-mean-squared fluctuation (see the Supporting Material); no noticeable features or differences between the I- and S-states were found.

I-State

The HZ molecule is oriented with its main axis along the bilayer normal direction, as reflected by the tilt angle fluctuating close to zero, of 22 ± 13° (mean ± SD). The rather broad distribution may be due to the flexibility of the structure of the molecule, which affects the helical axis direction within the simple definition employed here. HZ spans the region of hydrophobic lipid tails symmetrically, and the displacement of the COM of HZ from the center of the bilayer is 0.0 ± 1.7 Å (mean ± SD). Thus, HZ is only slightly mobile along the direction perpendicular to the bilayer surface.

One of the striking properties of the HZ molecule is its small length, and a meaningful question to ask is if and how such a short molecule may span the entire width of a lipid bilayer. Notably, the considered DMPC bilayer is a rather thin one: its hydrophobic thickness of ~25 Å in these simulations is well in the range of 23–27 Å found in the experimental literature (68–70). In the simplest idea of the peptide-bilayer interaction, the length of a hydrophobic peptide should match the hydrophobic thickness of the bilayer, to span the bilayer with no need for unfavorable interactions. To assess such a match, the length of the HZ molecule represented by the distance of the atoms Cα of Aib^{1} and $Leuol^{11}$ was measured. With the length of 17.6 ± 1.3 Å, HZ is only slightly longer in the I-state than in the S-state (16.3 ± 1.3 Å, mean ± SD); the corresponding distributions are shown in the Supporting Material. Apparently, the HZ molecule is too short to match the hydrophobic region of even such a thin bilayer as DMPC when immersed in the I-state.

Still, the polar termini of HZ might reach into the headgroup region of the bilayer if the bilayer is thinner in the vicinity of the HZ molecule; this would not be visible in the averaged density profiles in Fig. 2. To test this possibility, vertical density profiles were resolved by the horizontal distance from the COM of the HZ molecule (see Fig. 3). At distances above 15 Å, the thickness of the hydrocarbon tail region of 24–25 Å corresponds to the unperturbed value. In the range of 5–10 Å from the HZ molecule, however, the observed thickness decreased locally to ~20 Å, and is similar in the range below 5 Å. Thus, the hydrophobic region of the bilayer becomes thinner considerably in the vicinity of the HZ molecule. The termini of the HZ molecule in the I-state are capable of reaching into the lipid headgroup region and may participate in favorable interactions

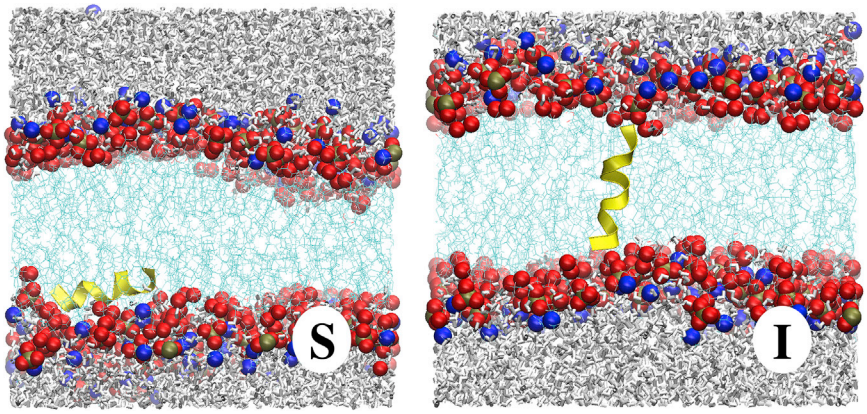

FIGURE 1 Given here are selected snapshots from free MD simulation, illustrating the two distinct orientations of the HZ molecule in a lipid bilayer that were observed: S-state (parallel to the surface, at its inner edge) and I-state (transmembrane, along the bilayer normal). To see this figure in color, go online.

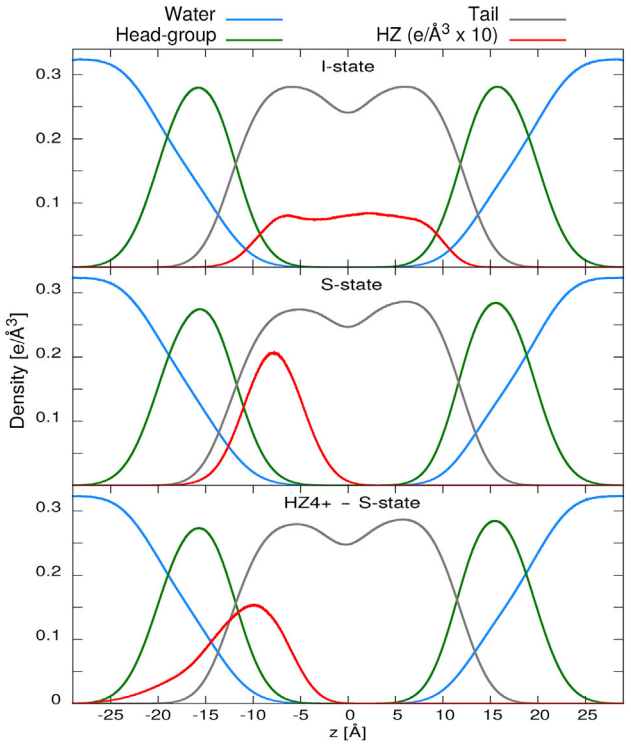

FIGURE 2 Given here are density profiles along the direction perpendicular to the bilayer plane, corresponding to the HZ molecule, water as well as the nonpolar tails and polar headgroups of the lipid. Electron density per unit volume (e/Å^3) is plotted for the I- and S-states of HZ as well as the S-state of the charged mutant HZ^{4+}. To see this figure in color, go online.

like H-bonding. The local thickness of bilayer with an HZ molecule in the S-state in presented in the Supporting Material for comparison.

Previously, it was reported that a rather thick D(22:1)PC bilayer thinned with added ALM, the long-sequence peptaibol (71), and a POPC bilayer thinned considerably in the vicinity of an inserted molecule of the lipopeptaibol trichogin GA IV (55). In this study, we have yet a different situation: there is a short-sequence peptaibol inserted into an inherently thin DMPC bilayer. Still, local thinning is observed, as an effort to reach a hydrophobic match of the inserted peptide and the hydrophobic thickness of the lipid bilayer.

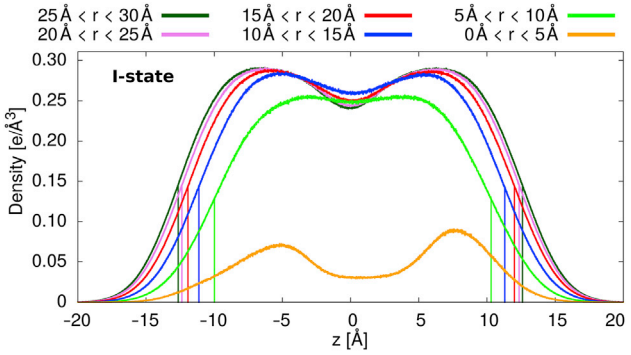

FIGURE 3 Given here are density profiles of the nonpolar hydrocarbon tails of DMPC in the simulation of HZ in the I-state. The different profiles were obtained considering lipid atoms in the given ranges of horizontal distances from the center-of-mass of the HZ molecule. (Horizontal distance is the distance projected in the plane of bilayer surface). To see this figure in color, go online.

S-State

A distinct observation is that the HZ molecule resides completely within the hydrophobic region of the bilayer, formed by the hydrophobic tails of the DMPC molecules. This is at odds with the usual behavior of amphiphilic membrane-active peptides, which often exhibit a strong interaction with the interface between the nonpolar and the polar regions due to the presence of one or more cationic amino acids (72). Such an effect is also observed in this study for the cationic mutant of HZ carrying four positive charges, HZ^{4+}. Compared with HZ, HZ^{4+} is located much further from the center of the bilayer, roughly at the polar/nonpolar interface. This is reflected by the observed distance of HZ^{4+} from the center of the bilayer of (11.5 $\pm$ 2.7) Å being significantly larger than (7.9 $\pm$ 1.7) Å for the uncharged HZ (mean $\pm$ SD). Let us rephrase this important observation: HZ is a strongly nonpolar peptide with no charged groups and few H-bonding donors or acceptors, and it is immersed nearly completely within the hydrophobic region of the bilayer, instead of interacting with the polar headgroups region in the way cationic peptides do.

Another structural feature of HZ is the orientation of the individual AA side chains, which describes the rotational state of HZ in the S-state along its helical axis. To this end, the z coordinate of the terminal heavy atom of each of the AA side chains (relative to the z coordinate of the COM of the HZ molecule) was calculated. These data, presented in Fig. 4, show which AA side chains point toward the hydrophobic volume preferentially, and which tend to interact with polar interface. Three of the five nonpolar side chains (Ile^4, Leu^7, and Leu^8) point toward the

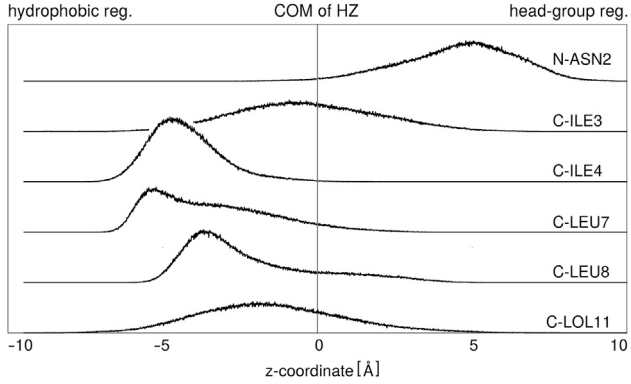

FIGURE 4 Shown here is the z coordinate of the terminal heavy atoms of the AA side chains except Aib and Pro. The value $z = 0$ corresponds to the center of mass of the HZ molecule; the side chain points toward the polar lipid headgroups if $z > 0$, whereas it points into the hydrophobic tail region if $z < 0$.

hydrophobic membrane region on average, and the two remaining ones (Leuol[11] and Ile[5]) are rather indifferent. By contrast, the only polar side chain (Asn[2]) points clearly toward the headgroups of the lipid. Note that the system is dynamic, and it would be wrong to expect all of the AA side chains to assume the described orientation for 100% of the time. On the other hand, the clear shape of the distributions obtained from an MD trajectory of 1 μs indicates that the result may be considered converged.

Experimental findings on the orientation of HZ in the bilayer

To provide experimental evidence in support of further MD analysis, we have performed biophysical characterization of the HZ in oriented zwitterionic bilayers and membrane mimics (unpublished data). We used ssNMR and synchrotron radiation circular dichroism (SRCD)—a combination of methods that is well established to experimentally characterize both overall conformation and orientation of α-helically folded membrane-active peptides (73–75). As can be seen in Fig. 5 *A*, HZ in 50% TFE (*black trace*) reveals CD spectrum with pronounced two negative bands at 205 nm (Band I) and ~220 nm (Band II) and a positive signal at ~190 nm. In general, this spectral shape corresponds to an overall helical fold but does not resemble continuous canonical secondary structure features of simple folds like α-helix, β-strand, random coil, poly-proline helix, etc. This appearance is closest to the spectra reported for 3_{10}-helically folded peptaibols and related model peptides composed of α-tetrasubstituted amino acids (76,77), in that 1) Band I is shifted to a lower wavelength than in an α-helix (205 nm instead of 208 nm) and 2) the Band I/Band II ratio is >1. However, quantitative deconvolution of the SRCD data using the DICHROWEB server (78) and a 3_{10}-helix containing dataset (Set 2, data between 178–260 nm) (78,79) does not reveal any significant amount of 3_{10}-helix (8.4–10%, depending on the algorithm used). On the contrary, in these deconvolutions, α-helix and random coil fractions spear to prevail (with 28.6–35% and 29–34.7%, respectively). Although being impossible to quantitatively assess the amount of β-bend ribbon conformation—because there is no corresponding CD model available—this latter result suggests another possibility for the interpretation of the CD spectrum: HZ could be structured as a mixture of, e.g., α-helical/3_{10}-helix in the middle of the sequence, and a random coil/extended fold toward molecular termini.

The orientation of an α-helix in an OCD spectrum is easy to determine by analyzing the intensity at the fingerprint wavelength of 208 nm; in the used sample arrangement, positive ellipticities should indicate the I-state and negative values correspond to the S-state orientation (75). Because HZ is not folded as an α-helix, its Band I does not fit 208 nm, but the fact that irrespective of the bilayer composition, the spectral shape stays unchanged, and, besides, resembles the isotropic solution spectrum, allows us to suggest S-state alignment from the SROCD data. This result is further supported by ssNMR experiments (see Fig. 5 *B*). From the ^{31}P-NMR, a high degree of bilayer alignment (>70% lipid are oriented) is visible, and no significant bilayer disruption is seen for the HZ reconstituted at 1 mol %. Because the sample preparation for SROCD and

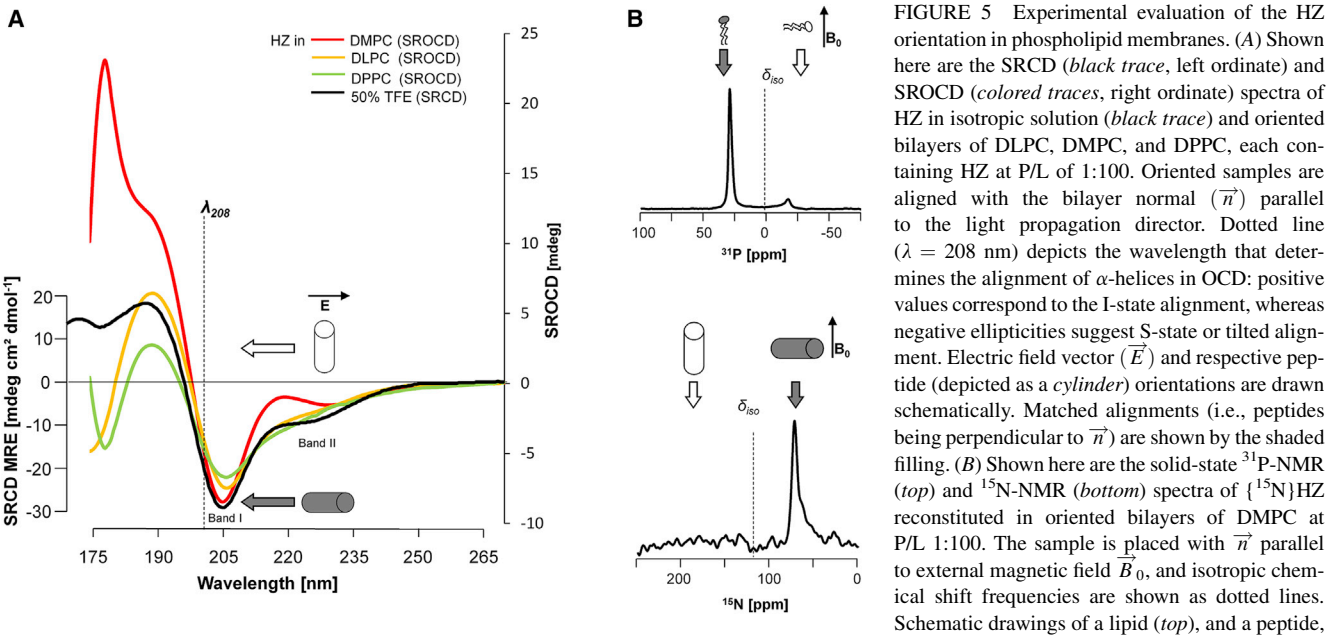

FIGURE 5 Experimental evaluation of the HZ orientation in phospholipid membranes. (*A*) Shown here are the SRCD (*black trace*, left ordinate) and SROCD (*colored traces*, right ordinate) spectra of HZ in isotropic solution (*black trace*) and oriented bilayers of DLPC, DMPC, and DPPC, each containing HZ at P/L of 1:100. Oriented samples are aligned with the bilayer normal ($\vec{n}$) parallel to the light propagation director. Dotted line (λ = 208 nm) depicts the wavelength that determines the alignment of α-helices in OCD: positive values correspond to the I-state alignment, whereas negative ellipticities suggest S-state or tilted alignment. Electric field vector ($\vec{E}$) and respective peptide (depicted as a *cylinder*) orientations are drawn schematically. Matched alignments (i.e., peptides being perpendicular to $\vec{n}$) are shown by the shaded filling. (*B*) Shown here are the solid-state ^{31}P-NMR (*top*) and ^{15}N-NMR (*bottom*) spectra of {^{15}N}HZ reconstituted in oriented bilayers of DMPC at P/L 1:100. The sample is placed with $\vec{n}$ parallel to external magnetic field $\vec{B}_0$, and isotropic chemical shift frequencies are shown as dotted lines. Schematic drawings of a lipid (*top*), and a peptide, depicted as a cylinder (*bottom*), demonstrate alignments with regard to $\vec{B}_0$, to which observed chemical shift anisotropy signal may correspond. Matched alignments (i.e., lipids being parallel and peptides being perpendicular to $\vec{n}$ and $\vec{B}_0$) are shown by the shaded filling. To see this figure in color, go online.

ssNMR is nearly identical, a similar degree of membrane alignment is expected in CD samples. Moreover, in the ^{15}N-NMR spectra no powder signals could be detected, suggesting no aggregation of the peptide. The selectively labeled HZ demonstrates instead chemical shift of 98 ppm, a clearly coplanar orientation of the HN-COO vector localized in the middle of HZ sequence (at Leu^{7}).

Taken together, SRCD and ssNMR data strongly suggest an S-state alignment of HZ in DMPC, but the conformational ambiguity is unresolved. The question of HZ structure remains to be answered either in a more detailed experimental study or by MD.

Structure of HZ from MD simulations

The structural ensembles of HZ were assessed. Besides the general goal, to characterize the conformation of the molecule, a specific question was whether HZ assumes a β-bend ribbon (spiral), which can be considered a subclass of the 3_{10}-helical family. To this end, a structural analysis was performed for the MD trajectories of HZ inserted in the DMPC bilayer both in the S-state and the I-state. A Ramachandran plot was obtained separately for each of the AAs 3–10 in both MD trajectories (see Fig. 6), which also shows the averaged structures of HZ from the unrestrained simulations in the S- as well as I-states.

The distributions of (φ,ψ) of both Leu and of both Ile are rather broad, located in the helical region of the plot. There is also a certain overlap with the typical β-bend values; note here the large fluctuation of the values reported in Ségalas et al. (19), reprinted in Table 1. The (φ,ψ) distributions for Aib and Pro are more distinct, located along the line typical for 3_{10}-helices, and there is also a certain match with the β-bend for Pro and a modest one for Aib. In short, no clear

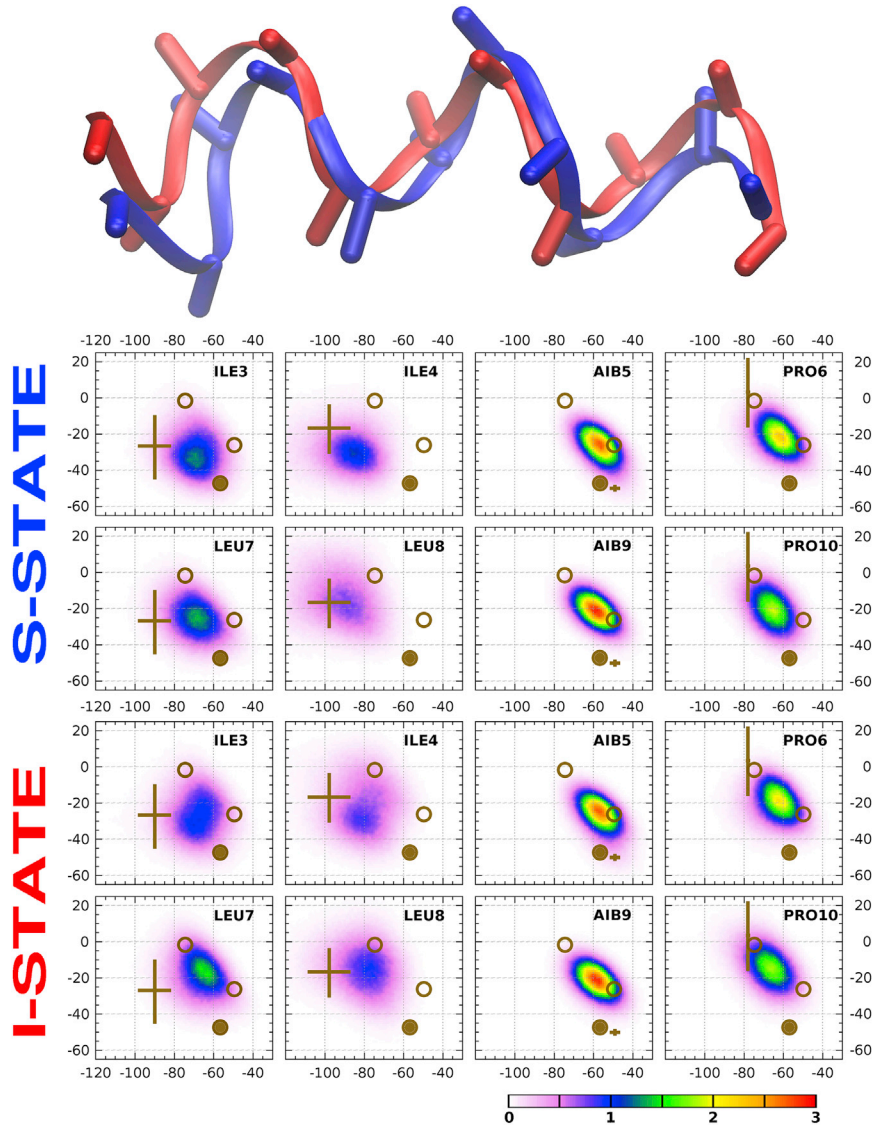

FIGURE 6 (*Top*) Given here are dominant conformations of the HZ molecule in the S-state (*blue/dark*) and the I-state (*red/light*). Structures were obtained with a PCA procedure run on MD trajectories, described in the Supporting Material. (*Bottom*) Given here are the Ramachandran plots for amino acids 3–10 of the HZ molecule interacting with a DMPC bilayer, in the S-state and in the I-state. The usual convention is employed (*horizontal axis*, φ and *vertical axis*, ψ, both in degrees); open circles, 3_{10}-helical conformations with ($-74°$, $-4°$) and ($-49°$, $-26°$); solid circles, α-helical conformation with ($-57°$, $-47°$); the locations and sizes of crosses represent the ranges reported for the β-bend ribbons in Ségalas et al. (19). See the Supporting Material for numerical values of (φ,ψ) of the dominant conformations. To see this figure in color, go online.

conclusion on the conformation of HZ is possible based on the analysis of Ramachandran plots; it may only be stated that the conformations of HZ in the S- and I-states seem to be similar. The structures of HZ accumulated along the MD trajectories were also compared to static, idealized conformations by means of the root-mean-squared displacements of atomic positions (see the Supporting Material). The root-mean-squared displacement values with respect to β-bend ribbon as well as 3_{10}-helix are low, indicating a large similarity to the idealized structures, whereas α-helical conformation is less likely.

Just one conformational element that differs between HZ in the S- and I-states is apparent in the Ramachandran plots as well as visually in the averaged structures. The Ramachandran plots show ψ of Leu^7 and φ of Leu^8 to be shifted clearly if slightly, by $\sim 15^\circ$ (whereas ψ of Leu^3 is shifted to an even lesser extent, by $\sim 10^\circ$). Accordingly, the average structures of HZ in the S- and I-states differ at the position 7–8. Apart from these particular features, few conformational distinctions are apparent.

Additional information on the structure of the HZ helix may be provided by the analysis of intrabackbone H-bonding patterns. To this end, lengths of putative backbone H-bonds typical of a 3_{10}-helical conformation were measured, and their distributions were obtained (see Fig. 7 (*left*)). Also here, there are very similar pictures of H-bonding for the HZ molecule in the S and I-states. Most

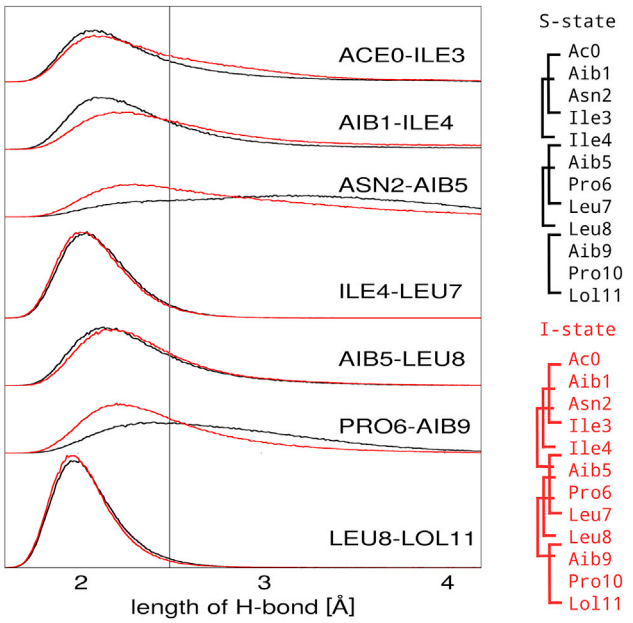

FIGURE 7 (*Left*) Shown here is the distribution of lengths of putative backbone hydrogen bonds in HZ, corresponding to the 3_{10}-helical conformation, in the S-state (*black/dark*) and in the I-state (*red/light*). ResX-ResY is the distance between the carboxy-O atom of ResX and the imino-H atom of ResY. The vertical line at 2.5 Å is a guide to the eye. (*Right*) Shown here are H-bonds present in the HZ molecule in the S and I-states. To see this figure in color, go online.

of the monitored putative H-bonds exhibit a distribution of length located close to 2 Å, showing good, stable H-bonding. However, two of the putative H-bonds, $Asn^2 \leftarrow Aib^5$ and $Pro^6 \leftarrow Aib^9$, show distributions that are shifted to longer distances in the S-state, meaning that these H-bonds cease to exist over certain periods of the respective MD trajectory. A qualitative picture of H-bonding in the HZ molecule in the S- and I-states that follows is presented in Fig. 7 (*right*).

In the I-state, there is a continuous pattern of $i \leftarrow i+3$ H-bonding along the entire HZ molecule, except the cases where a proline cannot be a hydrogen donor. By contrast, two more H-bonds are missing in HZ in the S-state: $Asn^2 \leftarrow Aib^5$ and $Pro^6 \leftarrow Aib^9$. Strikingly, this observation correlates with the idea of two possible β-bends of the type Xaa-Yaa-Aib-Pro stretching over the residues Ile^3–Pro^6 and Leu^7–Pro^{10}. These two bends might constitute rather independent structural elements, with a flexible mutual arrangement. Thus, a β-bend ribbon conformation is possible for the HZ molecule in the S-state, whereas the conformation is rather 3_{10}-helical in the I-state.

The sampling of structural ensembles is a persistent issue in MD simulations of lipid bilayer systems. Therefore, a procedure based on the principal component analysis (PCA) was employed to examine the convergence in the MD trajectories of HZ in the S- and I-states. The results are detailed in the Supporting Material. In a nutshell, the convergence of structural ensembles of HZ on the simulated timescale of 1 μs was confirmed.

To summarize, the structure of HZ immersed in a DMPC bilayer was characterized. The interpretation shall concentrate on the structure in the S-state, which was revealed as the more likely orientation by the experimental study. The I-state, which may be an intermediate in, e.g., the oligomerization of HZ, shall also serve as a reference to accessible structural space. The Ramachandran analysis corroborated what a simple visual inspection indicated, namely that the molecule assumes a structure in the 3_{10}-helical family, and a tendency to form a β-bend ribbon was confirmed by the analysis of H-bonding. The Leu^7-Leu^8 segment was shown to be flexible: while it assumes a rather stretched conformation in the (less likely) I-state orientation, it is bent slightly in the dominant S-state orientation.

Free energies from replica exchange simulations

The HREX method was employed to determine the relative free energies of the different orientations of the HZ molecule in a DMPC bilayer. Within the HREX framework, the force-field contributions localized in the HZ molecule were scaled down in all but one of the eight replicas of the molecular complex. The starting structure in all replicas of the HREX simulation had the HZ molecule inside the bilayer, perpendicular to the bilayer plane, i.e., close to the I-state, and the HZ molecule remained within the bilayer

for the entire simulation time of 2 μs. The resulting surface of free energy as a function of two variables—the z coordinate of the COM of HZ relative to the COM of bilayer, and the tilt angle between the long axis of HZ and the z axis—is presented in Fig. 8.

A pair of each of the two structures, the S- and I-states, observed in free simulations, are visible in the free energy plot clearly. Both of the S-states at $z \approx \pm 8$ Å and tilt angle of $\sim 90^\circ$ are equally deep global minima of energy; they are set to zero free energy in Fig. 8. The I-states at $z = 0$ and tilt of 15° and 165° are secondary minima, which lie higher in energy than those corresponding to the S-states. Because both leaflets of the bilayer are equivalent, the I-state minima should be equally deep much like the S-state minima, therefore we consider this feature of the plot not converged. An achievement to be appreciated is that the global minima have been reproduced, and the secondary minima are present and higher in energy. Although this simulation of 2 μs already sampled several interconversions between the S- and I-states, an extension of the simulation would be necessary to have the secondary minima converged as well. A conclusion that may be made at this point is that both the S-state and the I-state have been confirmed as the relevant structures, with the S-state being the most likely structure, in accordance with the above experimental conclusion.

A technical point worth discussion is the efficiency of sampling with these HREX simulations. Recall that the difficult convergence is due to the very slow rearrangements of lipid hydrocarbon tails, leading to very slow equilibration in MD simulations. The idea of HREX is to reduce energy barriers by way of scaling down appropriate contributions to the force-field energy of the molecular system. Now, it is not obvious if the scaling of interactions involving a nonpolar molecule like HZ (with, prominently, nonpolar lipid components) may improve the rate of sampling or not. A typical application of HREX would rely on the weakening of polar interactions or rotational barriers, which both do not apply in this study. This may be the reason for the failure of HREX to provide largely improved sampling efficiency.

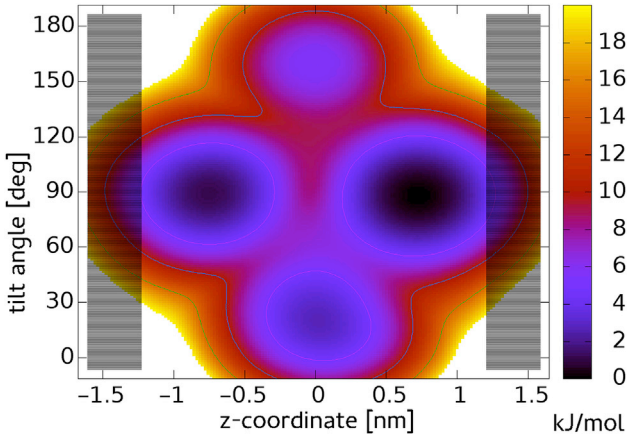

FIGURE 8 Given here is the free energy surface from the HREX simulation with an HZ molecule placed in the hydrocarbon tail region initially; shaded area indicates the region of polar lipid headgroups. To see this figure in color, go online.

An additional HREX simulation of 1 μs was performed with the HZ molecule placed in the aqueous phase initially, aiming at an estimate of the free energy profile of the HZ molecule passing from the solution to the bilayer (refer to the Supporting Material for a full report). There was, however, the problem that the HZ molecule only passed into the interior of the bilayer once, in a single HREX replica, during the microsecond simulation. Thus, it seems that obtaining convergence in such a simulation is far beyond the possibilities of current HREX methodology and computational equipment. The event of insertion that was observed may still constitute a starting point of a followup study of the mechanism of insertion. For the time being, we can merely state that the HZ molecule was inserted in the bilayer with its Leuol-terminus first (see Movie S1 in the Supporting Material). It has to be noted again that this event occurred once only, and took an amount of time that extended over several successful replica exchange instances; in other words, it took place in a simulation running with artificial and variant potential energy function.

DISCUSSION

We simulated a molecule of harzianin HK VI (HZ), a short-sequence peptaibol interacting with a DMPC bilayer. The goal was to assess the structure and orientation of HZ in the bilayer on the basis of unrestrained MD simulations. The simulations were complemented with ssNMR and SRCD experiments to facilitate a decision on the orientation. Further, it was attempted to estimate free energies from extended sampling simulations.

Two possible orientations of HZ in the bilayer were identified on the basis of free MD simulations: the I-state, with HZ perpendicular to the bilayer surface; and the S-state, where HZ lies in the hydrophobic part of the bilayer, close and parallel to its surface. The ensemble of simulations that were performed involved largely varying initial structures and orientations. Despite that, each of the simulations performed ended up in one of those two states. However, the sampling achieved in such free MD simulations was by far too insufficient to decide which of the orientations is preferred.

HREX simulations were performed to enhance the sampling of the different orientations of HZ in the bilayer. Even with this modern technique, however, it was still impossible to obtain a number of interconversions between the S- and I-states that would be sufficient to obtain conclusive results in terms of converged populations (or, equivalently, free energies). Calculation of free energies with extended metadynamics and umbrella sampling simulations

turned out to be even less practicable, as detailed in the Supporting Material.

The issue of unclear dominant orientation was resolved by means of ssNMR and SRCD experiments. Their analysis revealed that the HZ molecule is embedded in the surface of the bilayer preferably, i.e., it assumes the S-state. On the other hand, it is conceivable that the I-state may act as an important, low-energy intermediate in the insertion into bilayer, transfer between the bilayer leaflets, or in a process of aggregation of HZ into oligomers at conditions of higher P/L. Therefore, the following analysis of structure addressed both the S- and the I-state.

The structure of HZ, for which no hard experimental evidence is available, was characterized on the basis of free MD simulations. These were converged with respect to HZ structure, as confirmed by an analysis based on PCA. Ramachandran plots were inspected, and intrabackbone H-bonding patterns were investigated. The conformation of the HZ molecule in both the S- and I-state orientations falls into the 3_{10}-helical family. Apparently, the HZ molecule is somewhat longer along the helical axis in the I-state than in the S-state. This goes to the account of the slightly different conformation of the Leu^7-Leu^8 moiety.

In the more relevant S-state, the HZ molecule is located completely within the hydrophobic region of the bilayer, in contrast to the behavior of cationic amphiphilic peptides that usually dock into the hydrophobic/hydrophilic interface. In other words, HZ is immersed deeper into the bilayer than an amphiphilic peptide of comparable size. In addition, the HZ molecule in the S-state assumes an oriented rotational state: the polar side chain of Asn^2 is pointing toward the headgroup region, whereas the nonpolar side chains—all of the others except both Aib side chains—are oriented into the interior of the bilayer.

In the I-state, the HZ molecule is too short to match the hydrophobic thickness of an unperturbed DMPC bilayer. However, our analysis of local thickness profiles revealed that the HZ molecule present in the I-state induces a local thinning of the DMPC bilayer. Then, the length of the HZ molecule closely matches the (decreased) thickness of the hydrophobic region of the bilayer in the immediate vicinity of HZ. Therefore, although the S-state is the dominant orientation, the I-state may represent a conceivable, viable intermediate in processes like insertion or oligomerization of HZ.

This study illustrated the grand challenge of simulation of nonpolar peptides in lipid bilayers. Extended sampling techniques proved to be of limited use: HREX simulations, and even more so biasing potential methods (metadynamics and umbrella sampling simulations) hardly produced any useful results despite the large computational effort taken. Note that extremely low efficiency of umbrella sampling simulations of AMP binding was reported in Neale et al. (80). A viable alternative may be an application of a coarse-grained force field, which would require the secondary structure of HZ as an input for the parametrization. The results from this work could be used for this purpose, and we are currently working on an application for the oligomerization of HZ at elevated P/L.

SUPPORTING MATERIAL

Supporting Materials and Methods, Supporting Results, ten figures, one table, one movie, and one data file are available at http://www.biophysj.org/biophysj/supplemental/S0006-3495(17)30558-1.

AUTHOR CONTRIBUTIONS

S.A., S.L.G., T.B., A.S.U., and T.K. designed research. M.P. performed simulations. M.P., S.A., and T.K. analyzed simulations. S.K., A.B., G.C., and T.B. synthesized and purified the peptides. S.K. performed experiments with the help of S.A. and S.L.G. S.K., S.A., S.L.G., and A.S.U. analyzed experimental data. M.P., S.A., S.L.G., and T.K. wrote the article.

ACKNOWLEDGMENTS

This work was supported by the bwHPC Initiative and the bwHPC-C5 Project, funded by the state of Baden-Württemberg and the Research Foundation of Germany (DFG), through the services of the JUSTUS High Performance Computing Facility located at the University of Ulm, and further by the ANR-DFG grant 'Peptaibols' (DFG: UL 127/6-1), the Helmholtz Association program 'BIF-TM' and by the DFG (GRK 2039). We also acknowledge the ANKA CD-12 beamline as well as, personally, Jochen Bürck and Sigmar Roth.

SUPPORTING CITATIONS

References (81–96) appear in the Supporting Material.

REFERENCES

1. Leitgeb, B., A. Szekeres, …, L. Kredics. 2007. The history of alamethicin: a review of the most extensively studied peptaibol. *Chem. Biodivers.* 4:1027–1051.

2. Ruiz, N., G. Wielgosz-Collin, …, Y. F. Pouchus. 2007. New trichobrachins, 11-residue peptaibols from a marine strain of *Trichoderma longibrachiatum*. *Peptides.* 28:1351–1358.

3. Szekeres, A., B. Leitgeb, …, C. Vágvölgyi. 2005. Peptaibols and related peptaibiotics of Trichoderma. A review. *Acta Microbiol. Immunol. Hung.* 52:137–168.

4. Banerjee, R., S. Chattopadhyay, and G. Basu. 2009. Conformational preferences of a short Aib/Ala-based water-soluble peptide as a function of temperature. *Proteins.* 76:184–200.

5. Grubišić, S., B. Chandramouli, …, G. Brancato. 2016. Chain length, temperature and solvent effects on the structural properties of α-aminoisobutyric acid homooligopeptides. *Phys. Chem. Chem. Phys.* 18: 20389–20398.

6. Ueda, A., M. Oba, …, M. Tanaka. 2016. Helical structures of homochiral isotope-labeled α-aminoisobutyric acid peptides. *Tetrahedron.* 72:5864–5871.

7. Meyer, C. E., and F. Reusser. 1967. A polypeptide antibacterial agent isolated from *Trichoderma viride*. *Experientia.* 23:85–86.

8. Fox, R. O., Jr., and F. M. Richards. 1982. A voltage-gated ion channel model inferred from the crystal structure of alamethicin at 1.5-Å resolution. *Nature.* 300:325–330.

9. Mathew, M. K., and P. Balaram. 1983. A helix dipole model for alamethicin and related transmembrane channels. *FEBS Lett.* 157:1–5.
10. Wada, S., A. Iida, …, T. Fujita. 1996. Ion channel-forming property of trichorovin-XII, an 11-residue peptaibol from the fungus *Trichoderma viride*, in planar lipid bilayer membranes. *Bioorg. Med. Chem. Lett.* 6:2275–2278.
11. Mazzuca, C., L. Stella, …, B. Pispisa. 2005. Mechanism of membrane activity of the antibiotic trichogin GA IV: a two-state transition controlled by peptide concentration. *Biophys. J.* 88:3411–3421.
12. Rebuffat, S., S. Hlimi, …, B. Bodo. 1996. Isolation and structural elucidation of the 11-residue peptaibol antibiotic, harzianin HK VI. *J. Chem. Soc., Perkin Trans. 1*. 2021–2027.
13. Poirier, L., F. Quiniou, …, Y. F. Pouchus. 2007. Toxicity assessment of peptaibols and contaminated sediments on *Crassostrea gigas* embryos. *Aquat. Toxicol.* 83:254–262.
14. Antal, Z., L. Kredics, …, E. Nagy. 2005. Comparative study of potential virulence factors in human pathogenic and saprophytic *Trichoderma longibrachiatum* strains. *Acta Microbiol. Immunol. Hung.* 52:341–350.
15. Mikkola, R., M. A. Andersson, …, M. S. Salkinoja-Salonen. 2012. 20-Residue and 11-residue peptaibols from the fungus *Trichoderma longibrachiatum* are synergistic in forming Na^+/K^+-permeable channels and adverse action towards mammalian cells. *FEBS J.* 279:4172–4190.
16. Wada, S. I., and R. Tanaka. 2004. A novel 11-residual peptaibol-derived carrier peptide for in vitro oligodeoxynucleotide delivery into cell. *Bioorg. Med. Chem. Lett.* 14:2563–2566.
17. Wada, S., Y. Hitora, …, H. Urata. 2012. Cellular uptake of covalent conjugates of oligonucleotide with membrane-modifying peptide, peptaibol. *Bioorg. Med. Chem.* 20:3219–3222.
18. Schirmböck, M., M. Lorito, …, C. P. Kubicek. 1994. Parallel formation and synergism of hydrolytic enzymes and peptaibol antibiotics, molecular mechanisms involved in the antagonistic action of *Trichoderma harzianum* against phytopathogenic fungi. *Appl. Environ. Microbiol.* 60:4364–4370.
19. Ségalas, I., Y. Prigent, …, S. Rebuffat. 1999. Characterization of a type of β-bend ribbon spiral generated by the repeating (Xaa-Yaa-Aib-Pro) motif: the solution structure of harzianin HC IX, a 14-residue peptaibol forming voltage-dependent ion channels. *Biopolymers.* 50:71–85.
20. Kandt, C., W. L. Ash, and D. P. Tieleman. 2007. Setting up and running molecular dynamics simulations of membrane proteins. *Methods.* 41:475–488.
21. Lindahl, E., and M. S. P. Sansom. 2008. Membrane proteins: molecular dynamics simulations. *Curr. Opin. Struct. Biol.* 18:425–431.
22. Feller, S. 2001. Molecular Dynamics Simulation of Phospholipid Bilayers. Springer, Berlin, Germany, pp. 89–107.
23. Berendsen, H. J. C., and D. P. Tieleman. 2002. Molecular Dynamics: Studies of Lipid Bilayers. John Wiley & Sons, Hoboken, NJ.
24. Lyubartsev, A. P., and A. L. Rabinovich. 2016. Force field development for lipid membrane simulations. *Biochim. Biophys. Acta.* 1858:2483–2497.
25. Chipot, C., and A. Pohorille. 1997. Structure and dynamics of small peptides at aqueous interfaces: a multi-nanosecond molecular dynamics study. *J. Mol. Struct. THEOCHEM.* 398–399:529–535.
26. Chipot, C., and A. Pohorille. 1998. Folding and translocation of the undecamer of poly-L-leucine across the water-hexane interface. A molecular dynamics study. *J. Am. Chem. Soc.* 120:11912–11924.
27. Tieleman, D. P., H. J. C. Berendsen, and M. S. P. Sansom. 1999. Surface binding of alamethicin stabilizes its helical structure: molecular dynamics simulations. *Biophys. J.* 76:3186–3191.
28. Alecio, M. R., D. E. Golan, …, R. R. Rando. 1982. Use of a fluorescent cholesterol derivative to measure lateral mobility of cholesterol in membranes. *Proc. Natl. Acad. Sci. USA.* 79:5171–5174.
29. Tamm, L. K., and H. M. McConnell. 1985. Supported phospholipid bilayers. *Biophys. J.* 47:105–113.
30. Mills, R. 1973. Self-diffusion in normal and heavy water in the range 1–45°. *J. Phys. Chem.* 77:685–688.
31. Bond, P. J., J. Holyoake, …, M. S. P. Sansom. 2007. Coarse-grained molecular dynamics simulations of membrane proteins and peptides. *J. Struct. Biol.* 157:593–605.
32. Monticelli, L., S. K. Kandasamy, …, S.-J. Marrink. 2008. The MARTINI coarse-grained force field: extension to proteins. *J. Chem. Theory Comput.* 4:819–834.
33. Rzepiela, A. J., D. Sengupta, …, S.-J. Marrink. 2010. Membrane poration by antimicrobial peptides combining atomistic and coarse-grained descriptions. *Faraday Discuss.* 144:431–443, discussion 445–481.
34. Parton, D. L., E. V. Akhmatskaya, and M. S. P. Sansom. 2012. Multiscale simulations of the antimicrobial peptide maculatin 1.1: water permeation through disordered aggregates. *J. Phys. Chem. B.* 116:8485–8493.
35. Horn, J. N., T. D. Romo, and A. Grossfield. 2013. Simulating the mechanism of antimicrobial lipopeptides with all-atom molecular dynamics. *Biochemistry.* 52:5604–5610.
36. Lin, D., and A. Grossfield. 2014. Thermodynamics of antimicrobial lipopeptide binding to membranes: origins of affinity and selectivity. *Biophys. J.* 107:1862–1872.
37. Wang, Y., T. Zhao, …, J. P. Ulmschneider. 2014. How reliable are molecular dynamics simulations of membrane active antimicrobial peptides? *Biochim. Biophys. Acta.* 1838:2280–2288.
38. Gurtovenko, A. A., J. Anwar, and I. Vattulainen. 2010. Defect-mediated trafficking across cell membranes: insights from in silico modeling. *Chem. Rev.* 110:6077–6103.
39. Hub, J. S., B. L. de Groot, …, G. Groenhof. 2014. Quantifying artifacts in Ewald simulations of inhomogeneous systems with a net charge. *J. Chem. Theory Comput.* 10:381–390.
40. Sugita, Y., and Y. Okamoto. 1999. Replica-exchange molecular dynamics method for protein folding. *Chem. Phys. Lett.* 314:141–151.
41. Im, W., and C. L. Brooks, 3rd. 2005. Interfacial folding and membrane insertion of designed peptides studied by molecular dynamics simulations. *Proc. Natl. Acad. Sci. USA.* 102:6771–6776.
42. Nymeyer, H., T. B. Woolf, and A. E. Garcia. 2005. Folding is not required for bilayer insertion: replica exchange simulations of an α-helical peptide with an explicit lipid bilayer. *Proteins.* 59:783–790.
43. Vogel, A., M. Roark, and S. E. Feller. 2012. A reinterpretation of neutron scattering experiments on a lipidated Ras peptide using replica exchange molecular dynamics. *Biochim. Biophys. Acta.* 1818:219–224.
44. Li, J., R. Lakshminarayanan, …, R. W. Beuerman. 2012. Molecular dynamics simulations of a new branched antimicrobial peptide: a comparison of force fields. *J. Chem. Phys.* 137:215101.
45. Groot, R. D., and K. L. Rabone. 2001. Mesoscopic simulation of cell membrane damage, morphology change and rupture by nonionic surfactants. *Biophys. J.* 81:725–736.
46. Chen, L., N. Jia, …, L. Golubovic. 2013. Effects of antimicrobial peptide revealed by simulations: translocation, pore formation, membrane corrugation and Euler buckling. *Int. J. Mol. Sci.* 14:7932–7958.
47. Lin, D., and A. Grossfield. 2015. Thermodynamics of micelle formation and membrane fusion modulate antimicrobial lipopeptide activity. *Biophys. J.* 109:750–759.
48. Bereau, T., W. F. D. Bennett, …, M. Karttunen. 2015. Folding and insertion thermodynamics of the transmembrane WALP peptide. *J. Chem. Phys.* 143:243127.
49. Tieleman, D. P., M. S. P. Sansom, and H. J. C. Berendsen. 1999. Alamethicin helices in a bilayer and in solution: molecular dynamics simulations. *Biophys. J.* 76:40–49.
50. Tieleman, D. P., H. J. C. Berendsen, and M. S. P. Sansom. 2001. Voltage-dependent insertion of alamethicin at phospholipid/water and octane/water interfaces. *Biophys. J.* 80:331–346.
51. Tieleman, D. P., B. Hess, and M. S. P. Sansom. 2002. Analysis and evaluation of channel models: simulations of alamethicin. *Biophys. J.* 83:2393–2407.
52. Thøgersen, L., B. Schiøtt, …, E. Tajkhorshid. 2008. Peptide aggregation and pore formation in a lipid bilayer: a combined coarse-grained and all atom molecular dynamics study. *Biophys. J.* 95:4337–4347.

53. Násztor, Z., J. Horváth, and B. Leitgeb. 2013. Structural characterization of the short peptaibols trichobrachins by molecular-dynamics methods. *Chem. Biodivers.* 10:876–886.

54. Násztor, Z., J. Horváth, and B. Leitgeb. 2015. In silico conformational analysis of the short-sequence hypomurocin a peptides. *Int. J. Pept.* 2015:281065.

55. Bobone, S., Y. Gerelli, …, L. Stella. 2013. Membrane thickness and the mechanism of action of the short peptaibol trichogin GA IV. *Biochim. Biophys. Acta.* 1828:1013–1024.

56. Hornak, V., R. Abel, …, C. Simmerling. 2006. Comparison of multiple Amber force fields and development of improved protein backbone parameters. *Proteins.* 65:712–725.

57. Wickstrom, L., A. Okur, and C. Simmerling. 2009. Evaluating the performance of the ff99SB force field based on NMR scalar coupling data. *Biophys. J.* 97:853–856.

58. Maier, J. A., C. Martinez, …, C. Simmerling. 2015. ff14SB: improving the accuracy of protein side chain and backbone parameters from ff99SB. *J. Chem. Theory Comput.* 11:3696–3713.

59. Jämbeck, J. P. M., and A. P. Lyubartsev. 2012. Derivation and systematic validation of a refined all-atom force field for phosphatidylcholine lipids. *J. Phys. Chem. B.* 116:3164–3179.

60. Jämbeck, J. P. M., and A. P. Lyubartsev. 2012. An extension and further validation of an all-atomistic force field for biological membranes. *J. Chem. Theory Comput.* 8:2938–2948.

61. Jämbeck, J. P. M., and A. P. Lyubartsev. 2013. Another piece of the membrane puzzle: extending slipids further. *J. Chem. Theory Comput.* 9:774–784.

62. Jorgensen, W. L., J. Chandrasekhar, …, M. L. Klein. 1983. Comparison of simple potential functions for simulating liquid water. *J. Chem. Phys.* 79:926–935.

63. Berendsen, H. J. C., D. van der Spoel, and R. van Drunen. 1995. GROMACS: a message-passing parallel molecular dynamics implementation. *Comput. Phys. Commun.* 91:43–56.

64. Abraham, M. J., T. Murtola, …, E. Lindahl. 2015. GROMACS: high performance molecular simulations through multi-level parallelism from laptops to supercomputers. *SoftwareX.* 1–2:19–25.

65. Wang, Y., C. H. Chen, …, J. P. Ulmschneider. 2016. Spontaneous formation of structurally diverse membrane channel architectures from a single antimicrobial peptide. *Nat. Commun.* 7:13535.

66. Wang, L., R. A. Friesner, and B. J. Berne. 2011. Replica exchange with solute scaling: a more efficient version of replica exchange with solute tempering (REST2). *J. Phys. Chem. B.* 115:9431–9438.

67. Tribello, G. A., M. Bonomi, …, G. Bussi. 2014. PLUMED 2: new feathers for an old bird. *Comput. Phys. Commun.* 185:604–613.

68. Lewis, B. A., and D. M. Engelman. 1983. Lipid bilayer thickness varies linearly with acyl chain length in fluid phosphatidylcholine vesicles. *J. Mol. Biol.* 166:211–217.

69. Balgavý, P., M. Dubničková, …, D. Uhríková. 2001. Bilayer thickness and lipid interface area in unilamellar extruded 1,2-diacylphosphatidylcholine liposomes: a small-angle neutron scattering study. *Biochim. Biophys. Acta. Biomembr.* 1512:40–52.

70. Kučerka, N., Y. Liu, …, J. F. Nagle. 2005. Structure of fully hydrated fluid phase DMPC and DLPC lipid bilayers using x-ray scattering from oriented multilamellar arrays and from unilamellar vesicles. *Biophys. J.* 88:2626–2637.

71. Pan, J., D. P. Tieleman, …, S. Tristram-Nagle. 2009. Alamethicin in lipid bilayers: combined use of x-ray scattering and MD simulations. *Biochim. Biophys. Acta. Biomembr.* 1788:1387–1397.

72. Hong, M., and Y. Su. 2011. Structure and dynamics of cationic membrane peptides and proteins: insights from solid-state NMR. *Protein Sci.* 20:641–655.

73. Grage, S. L., S. Afonin, and A. S. Ulrich. 2010. Dynamic transitions of membrane-active peptides. *Methods Mol. Biol.* 618:183–207.

74. Wallace, B. A., and R. W. Janes. 2010. Synchrotron radiation circular dichroism (SRCD) spectroscopy: an enhanced method for examining protein conformations and protein interactions. *Biochem. Soc. Trans.* 38:861–873.

75. Bürck, J., P. Wadhwani, …, A. S. Ulrich. 2016. Oriented circular dichroism: a method to characterize membrane-active peptides in oriented lipid bilayers. *Acc. Chem. Res.* 49:184–192.

76. Toniolo, C., A. Polese, …, J. Kamphuis. 1996. Circular dichroism spectrum of a peptide 3_{10}-helix. *J. Am. Chem. Soc.* 118:2744–2745.

77. Formaggio, F., C. Peggion, …, C. Toniolo. 2004. Recent contributions of electronic circular dichroism to the investigation of oligopeptide conformations. *Chirality.* 16:388–397.

78. Whitmore, L., and B. A. Wallace. 2008. Protein secondary structure analyses from circular dichroism spectroscopy: methods and reference databases. *Biopolymers.* 89:392–400.

79. Janes, R. W. 2009. Reference datasets for protein circular dichroism and synchrotron radiation circular dichroism spectroscopic analyses. *In* Advances in Biomedical Spectroscopy, *1*. IOS Press, Amsterdam, the Netherlands, pp. 183–201.

80. Neale, C., J. C. Hsu, …, R. Pomès. 2014. Indolicidin binding induces thinning of a lipid bilayer. *Biophys. J.* 106:L29–L31.

81. Bürck, J., S. Roth, …, A. S. Ulrich. 2015. UV-CD12: synchrotron radiation circular dichroism beamline at ANKA. *J. Synchrotron Radiat.* 22:844–852.

82. Bayly, C. I., P. Cieplak, …, P. A. Kollman. 1993. A well-behaved electrostatic potential based method using charge restraints for deriving atomic charges: the RESP model. *J. Phys. Chem.* 97:10269–10280.

83. Frisch, M. J., G. W. Trucks, …, D. J. Fox. 2009. Gaussian 09 Revision C.01. Gaussian, Wallingford CT.

84. Darden, T., D. York, and L. Pedersen. 1993. Particle mesh Ewald—an n•log(*n*) method for Ewald sums in large systems. *J. Chem. Phys.* 98:10089–10092.

85. Gromacs. 2016. Gromacs Reference Manual, version 2016, section 4.9.1. http://manual.gromacs.org/documentation/2016/manual-2016.pdf, last accessed 7 Sep 2016.

86. Hess, B., H. Bekker, …, J. G. E. M. Fraaije. 1997. LINCS: a linear constraint solver for molecular simulations. *J. Comput. Chem.* 18: 1463–1472.

87. Nosé, S. 1984. A molecular dynamics method for simulations in the canonical ensemble. *Mol. Phys.* 52:255–268.

88. Hoover, W. G. 1985. Canonical dynamics: equilibrium phase-space distributions. *Phys. Rev. A.* 31:1695–1697.

89. Nosé, S., and M. L. Klein. 1983. Constant pressure molecular dynamics for molecular systems. *Mol. Phys.* 50:1055–1076.

90. Ulmschneider, J. P., J. C. Smith, …, E. Strandberg. 2012. Reorientation and dimerization of the membrane-bound antimicrobial peptide PGLa from microsecond all-atom MD simulations. *Biophys. J.* 103:472–482.

91. AmberTools. 2010. Amber Tools 1.4. http://ambermd.org.

92. Laio, A., and M. Parrinello. 2002. Escaping free-energy minima. *Proc. Natl. Acad. Sci. USA.* 99:12562–12566.

93. Barducci, A., G. Bussi, and M. Parrinello. 2008. Well-tempered metadynamics: a smoothly converging and tunable free-energy method. *Phys. Rev. Lett.* 100:020603.

94. Jämbeck, J. P. M., and A. P. Lyubartsev. 2013. Exploring the free energy landscape of solutes embedded in lipid bilayers. *J. Phys. Chem. Lett.* 4:1781–1787.

95. Bochicchio, D., E. Panizon, …, G. Rossi. 2015. Calculating the free energy of transfer of small solutes into a model lipid membrane: comparison between metadynamics and umbrella sampling. *J. Chem. Phys.* 143:144108.

96. Filipe, H. A. L., M. J. Moreno, …, L. M. S. Loura. 2014. How to tackle the issues in free energy simulations of long amphiphiles interacting with lipid membranes: convergence and local membrane deformations. *J. Phys. Chem. B.* 118:3572–3581.